A virtual photon energy fluence model for Monte Carlo dose calculation

Matthias Fippel,[a] Freddy Haryanto, Oliver Dohm, and Fridtjof Nüsslin
Abteilung für Medizinische Physik, Universitätsklinikum Tübingen, Hoppe-Seyler-Strasse 3, 72076 Tübingen, Germany

Stephan Kriesen
Klinik und Poliklinik für Strahlentherapie, Universität Rostock, Südring 75, 18059 Rostock, Germany

(Received 30 May 2002; accepted for publication 11 December 2002; published 5 February 2003)

The presented virtual energy fluence (VEF) model of the patient-independent part of the medical linear accelerator heads, consists of two Gaussian-shaped photon sources and one uniform electron source. The planar photon sources are located close to the bremsstrahlung target (primary source) and to the flattening filter (secondary source), respectively. The electron contamination source is located in the plane defining the lower end of the filter. The standard deviations or widths and the relative weights of each source are free parameters. Five other parameters correct for fluence variations, i.e., the horn or central depression effect. If these parameters and the field widths in the *X* and *Y* directions are given, the corresponding energy fluence distribution can be calculated analytically and compared to measured dose distributions in air. This provides a method of fitting the free parameters using the measurements for various square and rectangular fields and a fixed number of monitor units. The next step in generating the whole set of base data is to calculate monoenergetic central axis depth dose distributions in water which are used to derive the energy spectrum by deconvolving the measured depth dose curves. This spectrum is also corrected to take the off-axis softening into account. The VEF model is implemented together with geometry modules for the patient specific part of the treatment head (jaws, multileaf collimator) into the XVMC dose calculation engine. The implementation into other Monte Carlo codes is possible based on the information in this paper. Experiments are performed to verify the model by comparing measured and calculated dose distributions and output factors in water. It is demonstrated that open photon beams of linear accelerators from two different vendors are accurately simulated using the VEF model. The commissioning procedure of the VEF model is clinically feasible because it is based on standard measurements in air and water. It is also useful for IMRT applications because a full Monte Carlo simulation of the treatment head would be too time-consuming for many small fields.
 [DOI: 10.1118/1.1543152]

Key words: Monte Carlo, dose calculation, photon beam modeling

I. INTRODUCTION

Compared to conventional dose calculation methods (see, e.g., Ref. 1, and references therein) for radiation therapy treatment planning, Monte Carlo (MC) techniques[2–5] are potentially more accurate. The problem of fast and efficient MC simulation of photon and electron tracks within three-dimensional (3D) patient models has been solved in the last few years because of the increasing computing power and innovative variance reduction techniques.[6–14] An indispensable requirement for the accuracy of MC algorithms is an adequate model of the beam delivery system. That is, deviations between modeled and real particle fluence at the patient surface would propagate as dose distribution errors within the patient and the accuracy of the dose calculation algorithm can be lost.

There is an important advantage of the MC dose calculation technique: dose calculation within the patient (dose engine) can be decoupled completely from the treatment head model (fluence engine). Therefore, very different types of fluence engines can be employed, e.g., full MC simulations of the accelerator head or virtual source models based on analytical representations of the phase space distribution functions. Common to all fluence engines is just the capability of generating the parameters (energy, position, momentum) of photons and electrons in a phase space plane outside the patient according to the properties of the treatment head. This plane can then be used to start the MC transport of particle histories through the patient.

A clinically feasible Monte Carlo fluence engine should satisfy the following conditions:[10] (i) it should be simple enough to understand the behavior of the model, to have only a small number of free parameters, and to be fast in sampling the initial particle properties, (ii) the model parameters should be fixed by measurements that are not too complicated and time consuming (e.g., by measurements of profiles and depth dose curves in water and air), (iii) it should be complex enough to confirm all measurements in agreement with the accuracy demands. Full MC simulation of the whole accelerator head is one option to provide accurate photon and electron distributions in the phase space plane.[15–19] Another option is the construction of virtual source models based on these accelerator head simulations.[20–23] However, the required technical information and the time-consuming calculations limit its clinical feasibility. Therefore, virtual source

modeling with parameters fitted only from measured dose distributions in water and air is a third option to simulate at least the fluence contributions from the bremsstrahlung target, flattening filter, and primary collimator. An advantage of this third option is to exploit the experiences collected for the development of dual and triple source models for pencil beam, 3D convolution, and collapsed cone dose calculation algorithms.[24–35] In general, part of these models is a point source to simulate the primary photon component from the bremsstrahlung target. The head-scatter fluence has been modeled either by a second point source or by different spatial distribution functions. The precision of analytic models for MC dose calculation has been demonstrated already by comparison with measurement.[36]

The present paper introduces a virtual energy fluence (VEF) model of the photon beam head components above the collimating system. It is especially designed for Monte Carlo dose engines and it is solely based on measured dose distributions in water and air as well as some technical information from the linacs. Section II provides the details of the model and the commissioning procedure. In Sec. III comparisons to full MC accelerator head simulations and to measured dose distributions and output factors in water for Elekta and Siemens accelerators are shown. The XVMC code[10,11] is used for the calculation of dose in water.

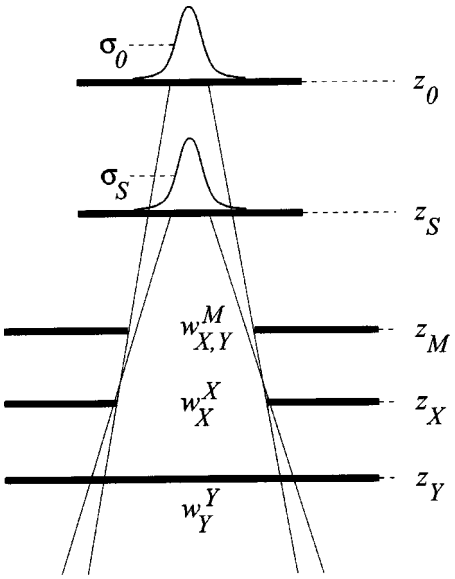

FIG. 1. Schematic representation of the VEF model for photon beams. The plane z_0 is the source of primary (target) photons, the plane z_S is the source of head-scatter (filter) photons and electron contamination. The location of the beam modifier plane z_M depends on the type of the linac. This shows an example with the modifier (MLC) above the jaws. Other examples are beam modifiers below the jaws or modifiers replacing one jaw pair. It is also possible to switch off the modifier plane in the VEF model.

II. MATERIAL AND METHODS

A. Geometry parameters of the sources

If we take into account the treatment head structure above the collimating system of conventional linear accelerators in a photon beam most of the radiation reaching the patient can be divided into three groups: (i) photons arising from the bremsstrahlung target (primary or target photons), (ii) photons scattering from the primary collimator and flattening filter (head-scatter or filter photons), and (iii) electron contamination. Therefore, the VEF model for Monte Carlo dose calculation (see Fig. 1) consists of photon and electron sources with relative contributions P_e for electrons and P_γ for photons satisfying the condition

$$P_e + P_\gamma = 1. \tag{1}$$

Usually, the amount of electron contamination P_e is small in clinical photon beams. Therefore the most important parts of the VEF model are the photon sources. The model presented here consists of two photon sources with relative contributions P_0 and P_S, where P_0 is for primary photons and P_S for head-scatter photons satisfying the condition

$$P_0 + P_S = 1. \tag{2}$$

The primary source is located in the bremsstrahlung target plane ($z = z_0$) and the scatter source is located in the flattening filter plane ($z = z_S$). Here, z corresponds to the distance from the virtual focus of the linac, which is not necessarily identical to the distance from target. z_0 and z_S can be estimated from the technical information of the linac treatment head, they are not fitted from measurements. Usually, for the primary source we use $z_0 = 0$, i.e., the virtual focus is located in the target plane. z_S is the distance from $z = 0$ to the lower boundary of the flattening filter. The initial photon positions are sampled from Gaussian distributions with standard deviations σ_0 and σ_S fitted from measurements. The nominal beam openings w^I_X and w^I_Y in the iso-center plane (the upper index I means iso-center and the lower indices X and Y represent the beam opening in the X and Y directions) are fixed in the beam defining planes given by $z = z_X$ and $z = z_Y$. Therefore, the beam openings in these planes are calculated by

$$w^X_X = w^I_X \frac{z_X}{z_I}, \quad w^Y_Y = w^I_Y \frac{z_Y}{z_I}. \tag{3}$$

Here, z_I is the distance to the iso-center (usually 100 cm). The parameters z_X and z_Y are also taken from the technical information of the linear accelerator. They are generally given by the lower limits of the X- and Y-jaw pairs or by the lower limit of the multileaf collimator (MLC) if one jaw pair is replaced by the MLC. To get the photon's X direction, we sample a second X position from a uniform distribution in the beam defining plane $z = z_X$, the Y direction is sampled from an uniform distribution in the plane $z = z_Y$. Since the assumption of uniform distributions is not correct, additional parameters are introduced in the following to correct the fluence profiles for the horn and/or central depression effects.

Since there are accelerators with two jaw pairs plus a MLC, we introduce one further plane $z = z_M$, called the beam modifier plane. The beam openings in this plane are given by

$$w^M_X = w^I_X \frac{z_M}{z_I}, \quad w^M_Y = w^I_Y \frac{z_M}{z_I}. \tag{4}$$

Using this information, the 3D photon fluence distribution of the primary source in air can be calculated by analytical integration of the Gaussian functions leading to a combination of error functions:

$$F_0(x,y,z)=\frac{(z_X-z_0)(z_Y-z_0)}{(z-z_0)^2}\,\frac{1}{4}\left\{\operatorname{erf}\left(\frac{x_0^+}{\sigma_0}\right)+\operatorname{erf}\left(\frac{x_0^-}{\sigma_0}\right)\right\}\left\{\operatorname{erf}\left(\frac{y_0^+}{\sigma_0}\right)+\operatorname{erf}\left(\frac{y_0^-}{\sigma_0}\right)\right\}. \tag{5}$$

The first term in Eq. (5) is necessary because of the inverse square law. The symbols x_0^+, x_0^-, y_0^+, and y_0^- are given by

$$\begin{aligned}
x_0^+&=\min\left(\frac{w_X^I z_X(z-z_0)+2xz_I(z_0-z_X)}{2\sqrt{2}z_I(z-z_X)},\frac{w_X^I z_M(z-z_0)+2xz_I(z_0-z_M)}{2\sqrt{2}z_I(z-z_M)}\right),\\
x_0^-&=\min\left(\frac{w_X^I z_X(z-z_0)-2xz_I(z_0-z_X)}{2\sqrt{2}z_I(z-z_X)},\frac{w_X^I z_M(z-z_0)-2xz_I(z_0-z_M)}{2\sqrt{2}z_I(z-z_M)}\right),\\
y_0^+&=\min\left(\frac{w_Y^I z_Y(z-z_0)+2yz_I(z_0-z_Y)}{2\sqrt{2}z_I(z-z_Y)},\frac{w_Y^I z_M(z-z_0)+2yz_I(z_0-z_M)}{2\sqrt{2}z_I(z-z_M)}\right),\\
y_0^-&=\min\left(\frac{w_Y^I z_Y(z-z_0)-2yz_I(z_0-z_Y)}{2\sqrt{2}z_I(z-z_Y)},\frac{w_Y^I z_M(z-z_0)-2yz_I(z_0-z_M)}{2\sqrt{2}z_I(z-z_M)}\right).
\end{aligned} \tag{6}$$

The min operators take into account the fact that the field widths are determined either by the jaw pairs or by an additional beam modifier (e.g., MLC) if the accelerator head consists of two jaw pairs plus the MLC. If, on the other hand, one jaw pair is replaced by the MLC then the min operations are unnecessary.

The corresponding fluence distribution of the head-scatter source is calculated by

$$F_S(x,y,z)=\frac{(z_X-z_S)(z_Y-z_S)}{(z-z_S)^2}\,\frac{1}{4}\left\{\operatorname{erf}\left(\frac{x_S^+}{\sigma_S}\right)+\operatorname{erf}\left(\frac{x_S^-}{\sigma_S}\right)\right\}\left\{\operatorname{erf}\left(\frac{y_S^+}{\sigma_S}\right)+\operatorname{erf}\left(\frac{y_S^-}{\sigma_S}\right)\right\}, \tag{7}$$

with

$$\begin{aligned}
x_S^+&=\min\left(\frac{w_X^I z_X(z-z_S)+2xz_I(z_S-z_X)}{2\sqrt{2}z_I(z-z_X)},\frac{w_X^I z_M(z-z_S)+2xz_I(z_S-z_M)}{2\sqrt{2}z_I(z-z_M)}\right),\\
x_S^-&=\min\left(\frac{w_X^I z_X(z-z_S)-2xz_I(z_S-z_X)}{2\sqrt{2}z_I(z-z_X)},\frac{w_X^I z_M(z-z_S)-2xz_I(z_S-z_M)}{2\sqrt{2}z_I(z-z_M)}\right),\\
y_S^+&=\min\left(\frac{w_Y^I z_Y(z-z_S)+2yz_I(z_S-z_Y)}{2\sqrt{2}z_I(z-z_Y)},\frac{w_Y^I z_M(z-z_S)+2yz_I(z_S-z_M)}{2\sqrt{2}z_I(z-z_M)}\right),\\
y_S^-&=\min\left(\frac{w_Y^I z_Y(z-z_S)-2yz_I(z_S-z_Y)}{2\sqrt{2}z_I(z-z_Y)},\frac{w_Y^I z_M(z-z_S)-2yz_I(z_S-z_M)}{2\sqrt{2}z_I(z-z_M)}\right).
\end{aligned} \tag{8}$$

The total photon fluence of both sources is then given by

$$F_\gamma(x,y,z)=P_0F_0(x,y,z)F_{\text{horn}}(x,y,z)+P_SF_S(x,y,z). \tag{9}$$

The expression $F_{\text{horn}}(x,y,z)$ corrects the primary photon fluence due to the horn or central depression effect. This effect is caused by the decreasing attenuation of the flattening filter with increasing distance to the central beam axis. $F_{\text{horn}}(x,y,z)$ is estimated by

$$F_{\text{horn}}(x,y,z)=1+\rho^2(h_0+h_1\rho+h_2\rho^2+h_3\rho^3+h_4\rho^4),$$

$$\text{with}\quad \rho=\frac{\sqrt{x^2+y^2}}{z-z_0}. \tag{10}$$

By convention the value of the horn correction parameter on the central axis ($\rho=0$) is unity and its derivative is zero. Motivated by accelerator head simulations using the BEAM Monte Carlo code,[16] we assume that it is unnecessary to correct the head-scatter fluence as well.

B. Generating the geometry parameters

Our intention is to fit the geometrical parameters P_0, σ_0, σ_S, h_0, h_1, h_2, h_3, and h_4 from measured profiles in air for different square and rectangular photon beams using an ionization chamber with build-up cap. For this reason, we first investigate the correlations between in-air dose, photon fluence, and energy. The direct proportionality of the photon

fluence $F_\gamma(x,y,z)$ and in-air dose $D_{\text{air}}(x,y,z)$ is obvious. However, the dependence of $D_{\text{air}}(x,y,z)$ on spectral or energy variations is not quite simple. To estimate this dependence, we have to know the photon energy spectrum as a function of x, y, and z. Because this is unknown here, we assume that the in-air dose distribution is fitted using Eq. (9) by replacing $F_\gamma(x,y,z)$ with $D_{\text{air}}(x,y,z)$ and multiplying the term on the right-hand side with a normalization factor N_F, i.e.,

$$D_{\text{air}}(x,y,z)=N_F\{P_0F_0(x,y,z)F_{\text{horn}}(x,y,z)+P_SF_S(x,y,z)\}. \tag{11}$$

When the beam commissioning process has finished we sample the initial photons for the MC dose calculation from the geometrical model derived from Eq. (11). However, we should have used Eq. (9) to fit the geometrical beam parameters. To take the difference between $D_{\text{air}}(x,y,z)$ and $F_\gamma(x,y,z)$ into account, we adjust the statistical weights of the sampled photons, which can be different from unity during MC simulations. That is, we sample the initial photon position and direction from the geometrical parameters. After that, we sample the photon energy from the spectrum function (see Sec. II C). With known photon energy we are able to estimate the ratio between $F_\gamma(x,y,z)$ and $D_{\text{air}}(x,y,z)$ (see Sec. II D) leading to the correct photon weight. The electron contamination P_e can be neglected for the in-air dose distributions because of the filtrating influence of the build-up cap.

In-air X, Y, and Z profiles must be measured for each energy and a variety of field sizes. Our experience is that the following field sizes provide a reasonable compromise between the measurement effort and the model accuracy: 2×2, 3×3, 5×5, 10×10, 20×20, 40×40, 5×40, 10×40, 40×5, and 40×10 cm^2. The following measurements should be performed:

(1) one Z profile (depth dose) at the central axis ($x=y=0$) from about $z=85$ cm to $z=115$ cm,
(2) three X profiles for $y=0$ and $z=85$ cm, $z=100$ cm, $z=115$ cm (alternative z values are possible),
(3) three Y profiles for $x=0$ and $z=85$ cm, $z=100$ cm, $z=115$ cm (alternative z values are possible),
(4) in-air output factors at $z=100$ cm for all field sizes normalized by one of the fields, usually the largest (40×40 cm^2).

The profiles must be normalized by the corresponding in-air output factors, 100% corresponds to the dose of a 40×40 cm^2 beam at the point $x=0$, $y=0$, $z=100$ cm. To take central axis deviations caused by measurement errors into account, it is useful to shift the profiles by the corresponding distance. This can generally be performed using the measurement (scanner) software. It might also be useful to symmetrize the measured profiles because Eq. (11) provides symmetric profiles. Indeed, it is much better if the accelerator is able to produce symmetric (or almost symmetric) and flat profiles. Symmetrization is also easily performed using standard water phantom software.

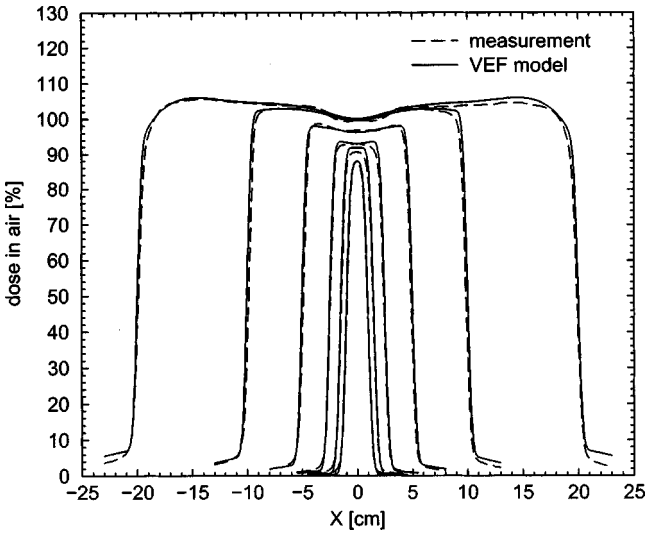

FIG. 2. Measured profiles in air (dashed lines) compared to the analytical representation of the fitted VEF model profiles (solid lines) of 2×2, 3×3, 5×5, 10×10, 20×20, and 40×40 cm^2 6 MV photon beams of a Siemens MD2 linear accelerator. The profiles in this example are measured with a source detector distance of 100 cm. Every profile is normalized using measured in-air output factors with the convention that 100% corresponds to the central axis dose of a 40×40 cm^2 field at 100 cm distance to the virtual source.

For fitting Eq. (11) to the normalized profiles, i.e., for calculating the parameters P_0, σ_0, σ_S, h_0, h_1, h_2, h_3, and h_4, a nonlinear χ^2 minimization algorithm based on the Levenberg–Marquardt method[37] is implemented. For this purpose, also the partial derivatives of Eq. (11) with respect to the parameters of the model are calculated analytically and implemented by the minimization algorithm. Figure 2 shows measured and fitted in-air profiles of a Siemens MD2 linear accelerator. This example demonstrates that the VEF model is able to predict central axis depressions as well as in-air output factors correctly. Only the output of the 3×3 cm^2 beam is slightly overestimated by the VEF model. Also the amount of fluence (in-air dose) outside the limits of the very large field (40×40 cm^2) is a little bit too large.

C. Energy behavior

Photon energy spectra of medical linear accelerators can be modeled by analytic functions with a few free parameters, e.g.,[10]

$$dEp(E)=dENE^l\exp(-bE),\quad E_{\min}\leqslant E\leqslant E_{\max}. \tag{12}$$

N is a normalization factor satisfying the condition:

$$\int_{E_{\min}}^{E_{\max}} dEp(E)=1. \tag{13}$$

$E_{\min}$ and $E_{\max}$ are the minimum and maximum photon energies. The most probable energy E_p and the mean energy $\langle E\rangle$ can be estimated from the free parameters l and b using the relationships:

$$E_p=\frac{l}{b},\quad \langle E\rangle\approx\frac{l+1}{b}. \tag{14}$$

The formula for $\langle E \rangle$ would be exact if we set the limits of integration in Eqs. (12) and (13) to $E_{\min}=0$ and $E_{\max}=\infty$.

Because of the shape of the flattening filter, the mean energy $\langle E \rangle$ of the spectrum decreases with increasing off-axis ray angle θ, i.e., with increasing distance to the central axis. Therefore, a correction method for this off-axis softening, based on measured half-value layer (HVL) data of water versus θ for various narrow photon beams,[38] is implemented. The idea is taken from a paper by Ahnesjö *et al.* where off-axis softening for superposition dose calculation has been described.[39] Figure 4 in Ref. 38 shows the ratio HVL(0)/HVL(θ) as a function of θ for different linear accelerators and nominal photon energies. This ratio is equivalent to the ratio of linear attenuation coefficients in water $\langle \mu(\theta) \rangle / \langle \mu(0) \rangle$ averaged over all energies of the spectrum. It has been shown in Ref. 38 that the data can be fitted by a third-degree polynomial:

$$\frac{\langle \mu(\theta) \rangle}{\langle \mu(0) \rangle} = \frac{\mathrm{HVL}(0)}{\mathrm{HVL}(\theta)} = 1 + 0.001\,81\theta + 0.002\,02\theta^2 - 0.000\,094\,2\,\theta^3. \quad (15)$$

To estimate the influence of Eq. (15) to the energy spectrum, we denote the off-axis energy distribution for ray angle θ by function $p(E_\theta, \theta)$ and the central axis spectrum by $p(E_0,0) \equiv p(E_0) \equiv p(E)$. E_θ is the photon energy sampled at ray angle θ. For simplicity we set the limits of integration to $E_{\min}=0$ and $E_{\max}=\infty$. Therefore, the normalization condition (13) becomes

$$\int_0^\infty dE_\theta\, p(E_\theta, \theta) = 1. \quad (16)$$

Now we assume that the off-axis spectrum can be calculated by scaling the central axis spectrum using the factor $s(\theta)$, i.e.,

$$p(E_\theta, \theta) = \frac{1}{s(\theta)} p\left(\frac{E_\theta}{s(\theta)}\right), \quad s(0)=1. \quad (17)$$

That is, during the MC simulation we sample E from $p(E)$ and in dependence on θ we get E_θ with

$$E_\theta = s(\theta) E. \quad (18)$$

To estimate the off-axis behavior of $s(\theta)$ we approximate the monoenergetic attenuation coefficient of water $\mu(E)$ using

$$\mu(E) = \mu_0 E^{-\nu}. \quad (19)$$

By averaging this attenuation coefficient we get

$$\langle \mu(\theta) \rangle = \frac{\mu_0}{s(\theta)} \int_0^\infty dE_\theta\, E_\theta^{-\nu} p\left(\frac{E_\theta}{s(\theta)}\right) = \mu_0 [s(\theta)]^{-\nu} \int_0^\infty dE\, E^{-\nu} p(E) \quad (20)$$

and therefore

$$\langle \mu(\theta) \rangle = [s(\theta)]^{-\nu} \langle \mu(0) \rangle, \quad \Rightarrow s(\theta) = \left[\frac{\langle \mu(0) \rangle}{\langle \mu(\theta) \rangle}\right]^{1/\nu}. \quad (21)$$

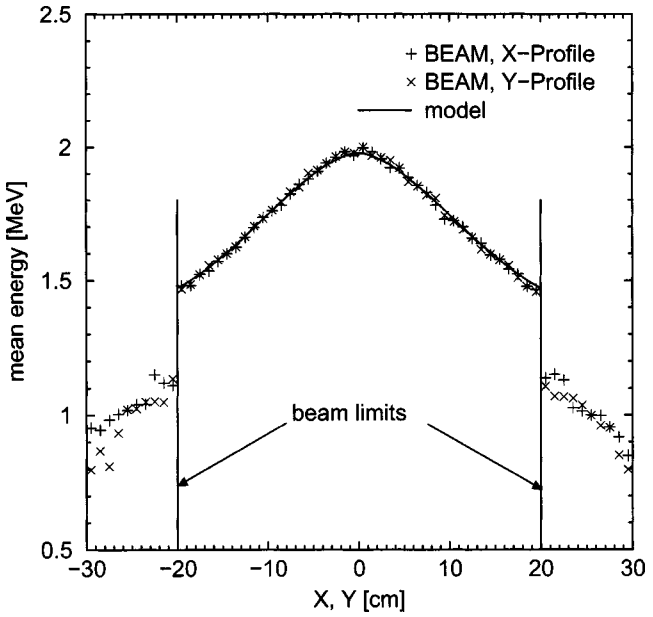

FIG. 3. Mean energy distributions of a 40×40 cm^2 6 MV photon beam simulated with BEAM for an Elekta SL*i* plus linear accelerator (dashed and dotted lines). The solid line represents the behavior of the analytic model based on HVL measurements.

It should be noted here, that this is a rough approximation. Furthermore, Eq. (15) has been derived by analyzing many types of linacs from various vendors with the exception of Elekta. Because in our clinic patients are treated using Elekta accelerators we wanted to be sure that our model is valid also for this type of machine. Therefore, we investigated the features of our linacs with the BEAM[16] MC code. One of the results of these studies is shown in Fig. 3. The plot shows the mean photon energy versus the distance to the central axis derived by analyzing the phase space file together with the prediction of the VEF model for $\nu=0.45$. This value of ν provides a reasonable fit of Eq. (19) to the monoenergetic attenuation coefficient in the energy range $0.2\,\mathrm{MeV} \leqslant E \leqslant 10\,\mathrm{MeV}$.[40] Figure 3 proves that the analytic off-axis softening model works also for Elekta linacs. Our results are consistent with a recent investigation by Sheikh-Bagheri and Rogers,[18] although they used a different Elekta accelerator type in their study.

To sample the central axis photon energy E from Eq. (12) a standard gamma distribution sampling routine[37] is used. Equation (18) corrects E to get the off-axis energy E_θ, however, only for primary photons (P_0). The energy of head-scattered photons (contribution P_S, which is typically on the order of 10%) is also sampled using Eq. (12), but this time corrected by

$$E \rightarrow \frac{E}{1+(1-\cos\phi)E/m_e}. \quad (22)$$

Here, m_e is the electron rest mass and ϕ the angle between the initial photon direction and the direction after scattering in the filter plane $z=z_S$, i.e., we assume Compton interactions within the flattening filter.

D. Relation between energy fluence and in-air dose

For the relationship between primary fluence $F_0(x,y,z)F_{\text{horn}}(x,y,z)$ and the corresponding in-air dose contribution $D_{\text{air},0}(x,y,z,E_\theta)$ of photons with energies between E_θ and $E_\theta + dE_\theta$ we assume

$$D_{\text{air},0}(x,y,z,E_\theta)dE_\theta \propto F_0(x,y,z)F_{\text{horn}}(x,y,z)E_\theta p(E_\theta,\theta)\mu_{\text{cap}}(E_\theta)dE_\theta. \quad (23)$$

It should be noted here that θ is a function of x, y, and z, i.e., $\theta=\theta(x,y,z)$. The inclusion of the factor E_θ on the right-hand side of Eq. (23) is motivated by the fact that the in-air dose is assumed to be proportional to the energy fluence, because Eq. (23) without the last term $\mu_{\text{cap}}(E_\theta)$ results in energy fluence. This last term (linear attenuation coefficient) takes into account the energy dependence of the build-up cap.

We want to calculate an off-axis correction factor, therefore we normalize Eq. (23) by the central axis dose contribution ($E_0 \equiv E$, $F_{\text{horn}}(0,0,z)=1$):

$$\frac{D_{\text{air},0}(x,y,z,E_\theta)dE_\theta}{D_{\text{air},0}(0,0,z,E)dE} = \frac{F_0(x,y,z)F_{\text{horn}}(x,y,z)}{F_0(0,0,z)}\frac{1}{w_E(\theta)} \quad (24)$$

with

$$\frac{1}{w_E(\theta)} \equiv \frac{E_\theta p(E_\theta,\theta)\mu_{\text{cap}}(E_\theta)dE_\theta}{Ep(E)\mu_{\text{cap}}(E)dE}. \quad (25)$$

That is, if we calculate the in-air dose contribution by Monte Carlo, we get a result different than the measurement because the energy correction $w_E(\theta)$ has been neglected during the commissioning of the geometry parameters (see Sec. II B). However, by multiplying the statistical photon weight by the factor $w_E(\theta)$ during the MC simulation we can reconstruct the measured curves. Substituting Eqs. (17) and (18) in Eq. (25) we get

$$w_E(\theta) = \frac{1}{s(\theta)}\frac{\mu_{\text{cap}}(E)}{\mu_{\text{cap}}(E_\theta)}. \quad (26)$$

To evaluate this formula we approximate the attenuation of the build-up cap by a fit to function:

$$\mu_{\text{cap}}(E) = \omega_0(E^{-\omega_1} + \omega_2 E). \quad (27)$$

If the unit of E is MeV we find for brass as build-up cap material in the energy range $0.2\,\text{MeV} \leqslant E \leqslant 15\,\text{MeV}$: $\omega_1 = 0.558$ and $\omega_2 = 0.026$.[40] Hence, the weighting factor becomes

$$w_E(\theta) = \frac{1}{s(\theta)}\frac{E^{-\omega_1}+\omega_2 E}{E_\theta^{-\omega_1}+\omega_2 E_\theta}. \quad (28)$$

For a given photon at position (x,y,z) the Monte Carlo procedure continues with sampling a central axis energy E from function $p(E)$. In dependence on the off-axis angle θ, the softening factor $s(\theta)$, the real photon energy E_θ, and the weighting factor $w_E(\theta)$ can be calculated, i.e., all parameters of the photon are fixed. The same build-up cap correction is applied to head-scatter photons (contribution P_S).

We found that the build-up cap correction is really necessary, especially to model dose distributions for large fields. The errors of dose predictions far off-axis can be 5% or larger if we neglect the sensitivity of the build-up cap material due to changes of the energy spectrum. On the other hand, the sensitivity of ionization chambers seems to be unimportant. To calculate corresponding correction factors we simulated the response of different ionization chambers using EGSNRC[5,41] and phase space files, generated with BEAM.[16] The corrections are on the order of 1% or below at least for our ionization chambers. In addition to it, if we measure profiles in water, we usually also neglect the influence of spectral variations to the ion chamber reading. Therefore, we did not take into account ion chamber corrections in the VEF model. For a more exact relation between energy fluence and dose in air and water further investigations will be necessary.

E. Electron contamination

Because for open photon beams the amount of electron contamination P_e is small compared to the contributions by photons (of the order of 1% or less), we approximate the electron source by a circular uniform distribution of electron starting points in the filter (or head-scatter) plane $z_e = z_S$. The radius R_e of the source is estimated by the flattening filter's footprint size. The electron direction is sampled in the same manner as the photon direction (see Sec. II A). Motivated by MC simulations using BEAM, the electron energy spectrum is modeled by an exponential distribution:

$$p(E_e)dE_e = N_e \exp\left(-\frac{E_e}{\langle E_e\rangle}\right)dE_e, \quad E_{\min} \leqslant E_e \leqslant E_{\max} \quad (29)$$

with the mean electron energy estimated by

$$\langle E_e\rangle \approx 0.13\ E_{\text{nom}} + 0.55\ \text{MeV}. \quad (30)$$

E_{nom} is the nominal voltage of the beam in MeV. The relative weight P_e of the electron source is determined by fitting a measured depth dose in water (see Sec. II F).

F. Generating the spectrum and electron parameters

One measured central axis depth dose curve of a 10×10 cm^2 beam per photon energy with a distance of the radiation source to the water phantom surface (SSD) of 100 cm (alternate field sizes or SSDs are possible) is required to deconvolve the photon energy spectrum and the amount of electron contamination. Therefore, a set of ''monoenergetic'' central axis depth dose distributions must be calculated using the MC dose engine, i.e., using XVMC in our case. Here, we use quotation marks to emphasize that the depth dose curves are not really monoenergetic, because Eqs. (18) and (22) are applied to correct the energy due to softening effects. Only the energy at the central axis is constant for a ''monoenergetic'' depth dose curve. Furthermore, the geometry parameters, generated as described in Sec. II B, are used to calculate the depth dose curves. The energy range should reach from 0.25 to 10 MeV for 6 MV photon beams and from 0.25 to 20 MeV for 15 MV photon beams. In addition to the

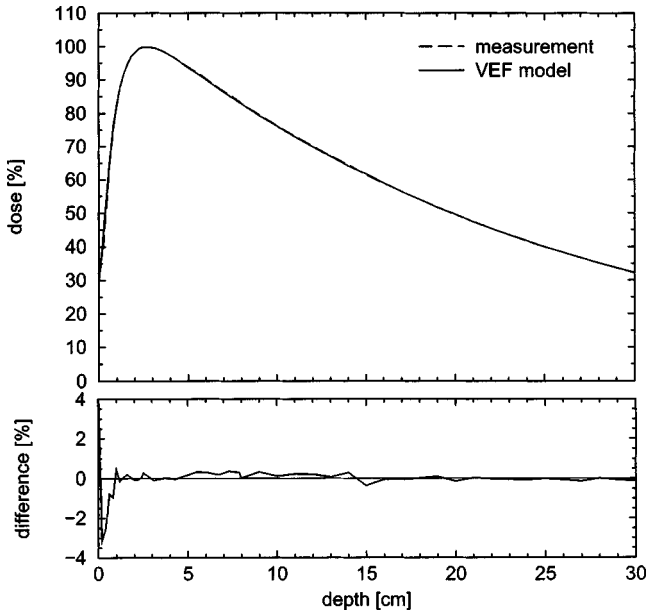

FIG. 4. Measured depth dose curve in water (dashed line in the upper plot) compared to the fitted VEF model depth dose curve (solid line in the upper plot) of a 10×10 cm^2 15 MV photon beam of an Elekta SL*i* plus linear accelerator. The SSD is 100 cm. The lower plot (solid line) shows the difference between measurement and the VEF model.

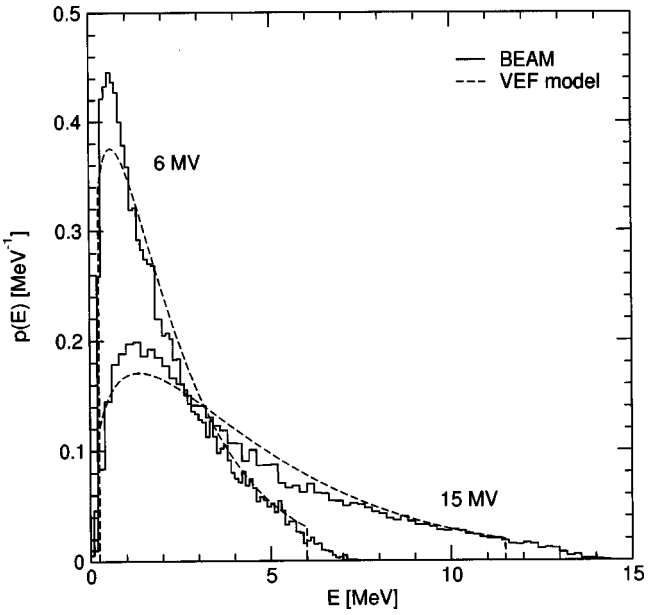

FIG. 5. 6 and 15 MV energy spectra of the primary (target) photon contribution at the central axis simulated with BEAM for an Elekta SL*i* plus linear accelerator (solid histograms) compared to the spectra derived by fitting central axis depth dose distributions using the VEF model (dashed lines). The spectra are normalized by the condition $\int dE\, p(E)=1$.

''monoenergetic'' photon depth dose curves, one electron depth dose curve has to be calculated using the estimated parameters z_e, R_e, and $\langle E_e\rangle$ from Sec. II E.

The MC simulations to calculate these depth dose curves must be performed with a model of the collimating system (jaws and MLC), because the measurements are influenced by the collimators. Here, a very simple MLC model may be sufficient, e.g., a ''cookie cutter'' model that rejects each particle outside the beam segment contour. For our investigations here we implement a more realistic model of the MLC based on Monte Carlo C++ classes for arbitrary geometries constructed from planes and other surfaces in 3D space. Therefore, it is possible to include effects caused by the rounded leaf ends and the tongue-and-groove design of our MLC. A description of theses geometry classes will be published in a future paper.

The next step of the commissioning procedure is to employ Eqs. (1), (12), and (29) with some estimated initial parameters P_e, l, b, and $E_{\max}$ (for $E_{\min}$ we usually use a fixed value of 0.25 MeV) for the superposition of the calculated depth dose curves. As in Sec. II B, a nonlinear χ^2 minimization algorithm based on the Levenberg–Marquardt method[37] is implemented to fit the superimposed depth dose curves and the measured curve. The upper plot in Fig. 4 shows a measured and a fitted depth dose curve in water of a 10×10 cm^2 15 MV photon beam of an Elekta SL*i* plus linear accelerator. The lower plot shows the difference between both curves after finishing the χ^2 minimization. The largest deviations can be observed near the water surface, but here the influence of measurement errors is not negligible and a large deviation in dose corresponds to a small shift in depth direction only. Figure 5 shows the resulting energy spectra for 6 and 15 MV photon beams compared to simulations using the BEAM code. The differences between simulated and fitted spectra are mainly caused by the special analytic form of Eq. (12). More parameters should improve the quality of the fit, but on the other hand, more degrees of freedom can cause multiple solutions of the fit problem. Therefore, we implement the energy spectrum of Eq. (12) in the VEF model.

We find that the amount of electron contamination P_e for our Elekta accelerators, derived in the manner described here, ranges from about 0.9% for 6 MV to about 1.5% for 15 MV photon beams. This corresponds to 6% and 11% surface dose, respectively. Similar results for Siemens machines are obtained. These observations are consistent with MC simulations using the BEAM code.[18]

III. RESULTS

The commissioning procedure is based on a variety of measurements in air but only on one depth dose curve in water for a defined field size, 10×10 cm^2 in the case described here. Therefore, additional measurements in water are useful to verify the model and the derived parameters. As examples, we present some of our comparisons between measurements in water and the corresponding Monte Carlo simulations for two types of linear accelerators.

Tables I and II show measured and calculated output factors (OFs) at 10 cm depth of water for Elekta and Siemens machines. The SSDs were 90 cm in Table I and 100 cm in Table II. The OFs are normalized relative to the corresponding 10×10 cm^2 fields. Apart from a few exceptions, the agreement between measured and calculated OFs is better than 2%. The largest disagreement (4.4%) is for the 2×2 cm^2 6 MV beam of the Siemens MD2 accelerator. However, for

TABLE I. Measured and calculated output factors (OFs) at 10 cm depth in water for an Elekta machine. The SSD is 90 cm and the OFs are normalized relative to the 10×10 cm^2 field. Note: the linacs from this Table and Fig. 6 are not identical.

Energy	Field size (cm^2)	Meas OF	Calc OF	Difference %
6 MV	2×2	0.792	0.806	1.4
	3×3	0.844	0.865	2.1
	5×5	0.903	0.916	1.3
	15×15	1.057	1.066	0.9
	20×20	1.099	1.094	0.5
	30×30	1.146	1.136	1.0
	40×40	1.167	1.158	0.9
15 MV	2×2	0.777	0.781	0.4
	3×3	0.857	0.885	2.8
	5×5	0.925	0.940	1.5
	15×15	1.043	1.042	0.1
	20×20	1.070	1.055	1.5
	30×30	1.099	1.085	1.4
	40×40	1.114	1.088	2.6

very small fields the influence of ion chamber volume on measured and voxel size on calculated dose may not be negligible.[42] This can also be observed in Fig. 6 where OFs measured with different detectors (ion chamber, pinpoint chamber, diamond detector, and diode detector) are compared to calculations with BEAMNRC and XVMC for a second Elekta SL*i* plus accelerator (note: the linacs from Table I and Fig. 6 are not identical). In contrast to Table I, here the SSD of the water phantom is 100 cm. Figure 6 shows that the VEF model overestimates slightly the output for fields

TABLE II. Measured and calculated output factors (OFs) at 10 cm depth in water for the Siemens MD2 accelerator. The SSD is 100 cm and the OFs are normalized relative to the 10×10 cm^2 field.

Energy	Field size (cm^2)	Meas OF	Calc OF	Difference %
6 MV	2×2	0.770	0.726	4.4
	3×3	0.828	0.837	0.9
	5×5	0.889	0.897	0.8
	5×20	0.965	0.971	0.6
	5×40	0.977	0.974	0.3
	10×40	1.068	1.068	0.0
	20×5	0.949	0.952	0.3
	20×20	1.102	1.116	1.4
	40×5	0.958	0.970	1.2
	40×10	1.051	1.065	1.4
	40×40	1.167	1.174	0.7
10 MV	2×2	0.767	0.743	2.4
	3×3	0.845	0.857	1.2
	5×5	0.909	0.919	1.0
	5×20	0.972	0.970	0.2
	5×40	0.983	0.979	0.4
	10×40	1.054	1.044	1.0
	20×5	0.957	0.962	0.5
	20×20	1.078	1.084	0.6
	40×5	0.962	0.972	1.0
	40×10	1.037	1.044	0.7
	40×40	1.123	1.129	0.6

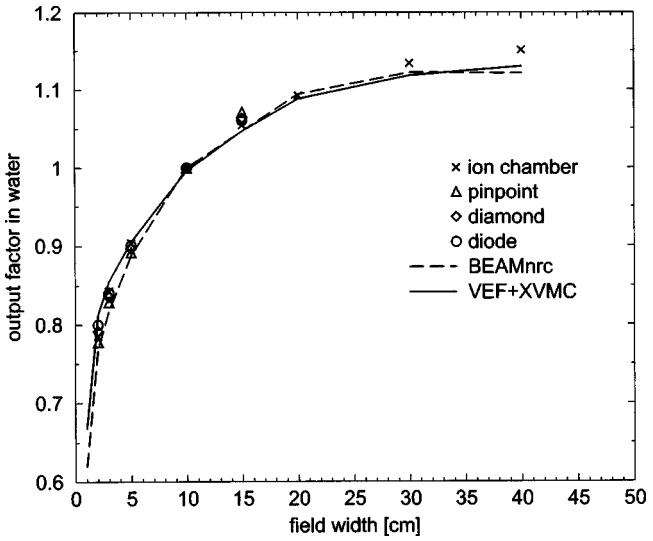

FIG. 6. Measured (ionization chamber, pinpoint chamber, diamond detector, and diode detector) vs calculated (BEAM and VEF model) output factors at 10 cm depth in water for 6 MV beams of an Elekta SL*i* plus linear accelerator. The SSD is 100 cm (different than Table I) and the OFs are normalized relative to the 10×10 cm^2 field. Note: the linacs here and in Table I are not identical.

smaller than 10×10 cm^2 but underestimates the output for very large fields. But on the other hand, the deviations to the ion chamber measurements are smaller than 2% for the majority of the field sizes. Only for the 2×2 cm^2 (2.8%) and 40×40 cm^2 (2.1%) beams the deviations are larger. Furthermore, the full MC simulation of the accelerator head (dashed line in Fig. 6) has problems in predicting the output for 30×30 and 40×40 cm^2 fields correctly. Therefore, more investigations will be necessary to discover the reasons for these disagreements.

Figures 7–9 show measured and calculated depth dose

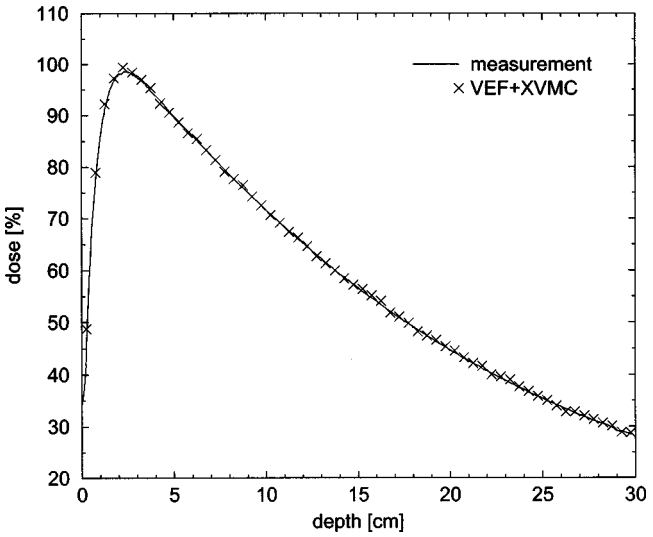

FIG. 7. Measured (solid line) compared to calculated depth dose distribution in water for a 10 MV 5×20 cm^2 photon beam of a Siemens MD2 linear accelerator. The SSD is 100 cm. The curves are normalized using the output factors from Table II with 100% corresponding to the maximum of a 10×10 cm^2 field in water, i.e., a comparison of absolute dose values is shown.

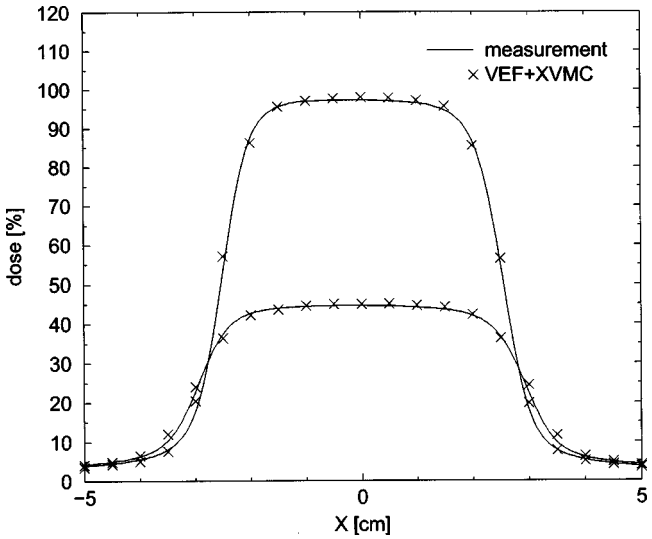

FIG. 8. Measured (solid lines) compared to calculated *X* profiles at 3 and 20 cm depths in water for the same example and with the same normalization as in Fig. 7.

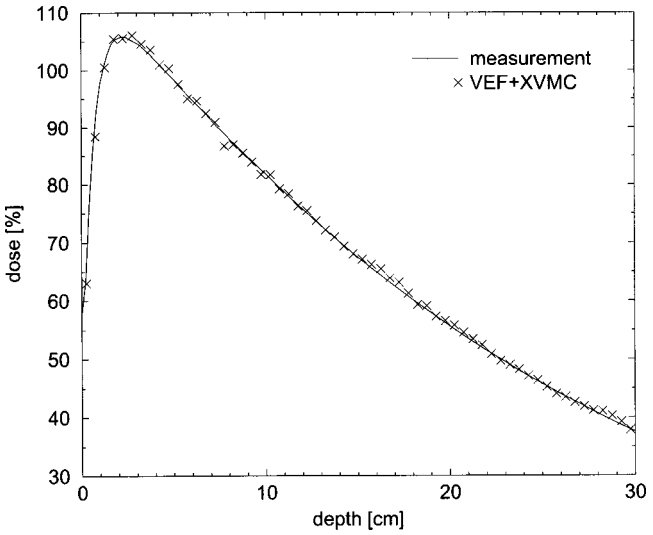

FIG. 10. Measured (solid line) compared to calculated depth dose curves in water for a 15 MV 30×30 cm^2 photon beam of an Elekta SL*i* plus linear accelerator. As in Fig. 7 dose values normalized by the 10×10 cm^2 output factor are shown.

curves and profiles in water for a 10 MV 5×20 cm^2 photon beam of the Siemens MD2 accelerator. The curves are normalized using the output factors from Table II with 100% corresponding to the maximum of a 10×10 cm^2 field in water, i.e., Figs. 7–9 show comparisons of absolute dose distributions. In particular, the profiles in Figs. 8 and 9 demonstrate that the VEF model is able to predict the horn effect as well as the dose outside the field limits in good agreement with measurement. Figures 10 and 11 are presented to validate the off-axis softening and charged particle contamination models for large field sizes (30×30 cm^2) and high energies (15 MV). One of the Elekta linacs is used for this comparison.

Figures 12–14 demonstrate the accuracy of the VEF model compared to MC simulations with full knowledge of the accelerator head design. Figures 12–14 show comparisons of profiles of 3×3 and 10×10 cm^2 6 MV photon beams −10 and +5 cm off-axis in water (SSD=100 cm) calculated with BEAMNRC (symbols) and XVMC using the VEF model (lines). The normalization is equivalent to Figs. 7–9, but this time for the Elekta machine of Table I. The statistical variance of the BEAM simulations is influenced by the limited size of the phase space files. The VEF model slightly overestimates the penumbra width. On the other hand, we find agreement especially within the field and outside the field limits. For a verification of the BEAM simulations by measurements, we refer to Ref. 42.

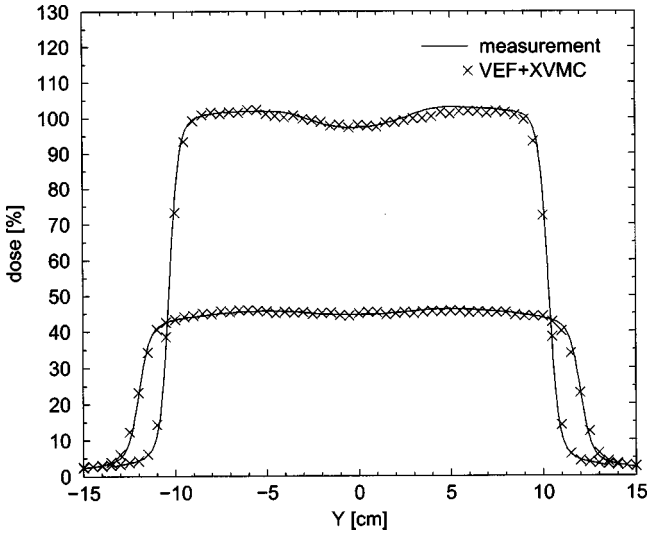

FIG. 9. Measured (solid lines) compared to calculated *Y* profiles at 3 and 20 cm depths in water for the same example and with the same normalization as in Fig. 7.

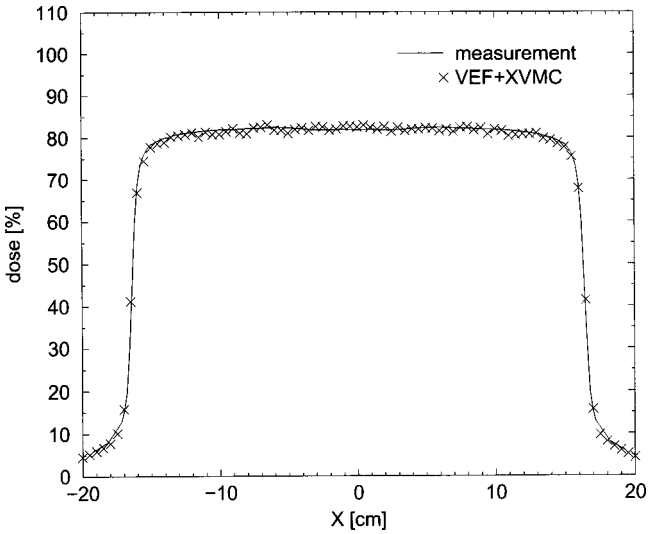

FIG. 11. Measured (solid line) compared to calculated *X* profiles at 10 cm depths in water for the example of Fig. 10.

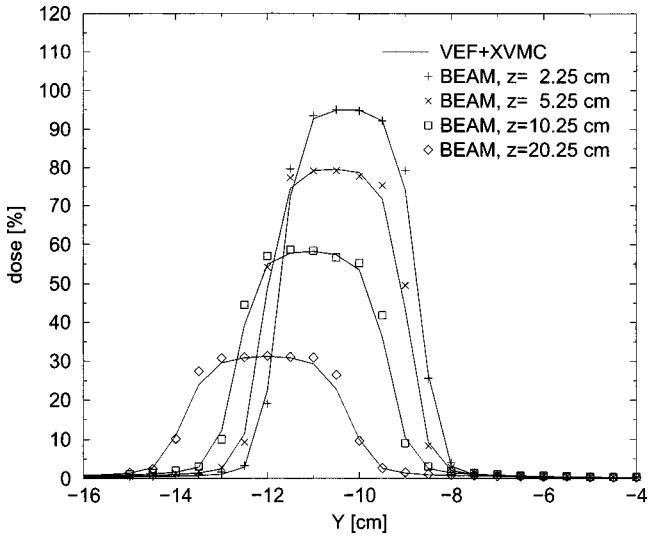

FIG. 12. Comparison of *Y* profiles in four different depths of a 3×3 cm^2 6 MV photon beam -10 cm off-axis in water (SSD=100 cm) calculated with BEAMNRC using the full information of the accelerator head (symbols) and XVMC using the VEF model (lines).

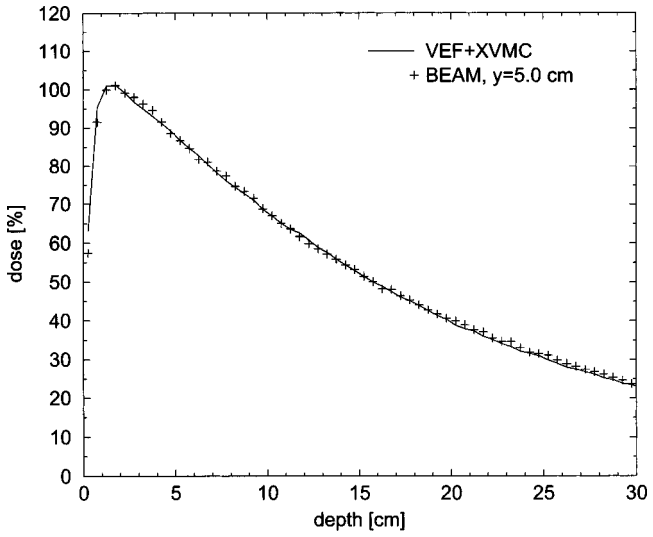

FIG. 14. Comparison of depth dose curves +5 cm off-axis in water for the example of Fig. 13.

IV. CONCLUSIONS

The purpose of the present paper is to introduce a treatment head model for Monte Carlo dose calculation that can be easily commissioned and implemented in clinical routine. Like beam models for conventional dose calculation algorithms, the virtual energy fluence model described here is based on standard measurements in water and air. Only a few parameters are required from the technical information of the accelerator. By comparison with results derived by the BEAMNRC software system, it is demonstrated that time-consuming MC simulations of the whole accelerator head are unnecessary for radiation therapy planning purposes.

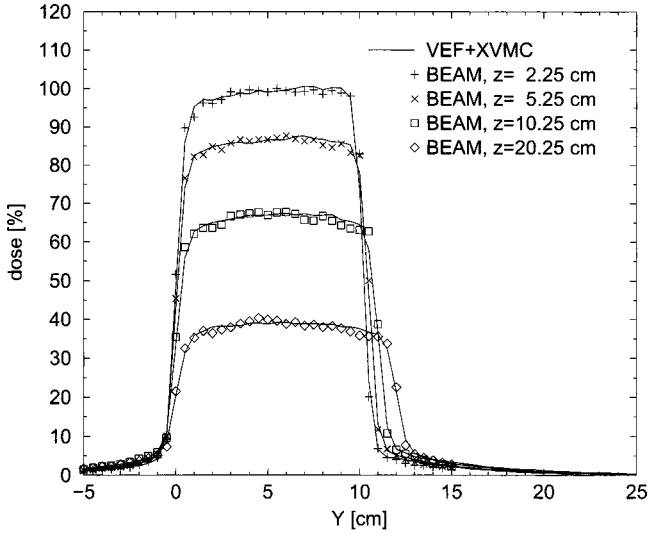

FIG. 13. Comparison of *Y* profiles in four different depths of a 10×10 cm^2 6 MV photon beam +5 cm off-axis in water (SSD=100 cm) calculated with BEAMNRC using the full information of the accelerator head (symbols) and XVMC using the VEF model (lines).

On the other hand, the VEF model should not be considered as a completed development. It is open for improvements and extensions. Especially the methods to compute and emulate the central axis energy spectrum are not in a final state. To get closer to MC generated spectra, more parameters of the analytical spectrum representations or tabulated spectra will be necessary. The problem is, however, that the calculated shape of the spectrum is not quite unique if it is deconvolved from measured depth dose curves. Measured depth dose curves in water are also prone to experimental setup errors and a small shift of the curve can result in a significant change of the spectrum. One possible solution to this problem could be that each vendor of medical linear accelerators provides the energy information of its machines.

The off-axis softening behavior of the central axis spectrum seems to be similar between most accelerators. For this type of machine the VEF model off-axis softening approach presented here will be sufficient.

An important additional result of this paper is that the influence of a build-up cap on the ion chamber signal cannot be neglected during in-air profile measurements. There might also be an influence of the ionization chamber itself. However, simulations using EGSNRC and BEAM have shown that this influence is smaller than 1%. Furthermore, this effect should, in the same manner, influence the profile verification measurements in water. Therefore, a corresponding correction is not implemented into the VEF model.

ACKNOWLEDGMENT

This work has been performed under the auspices of the Deutsche Forschungsgemeinschaft.

[a]Electronic mail: msfippel@med.uni-tuebingen.de

[1] A. Ahnesjö and M. M. Aspradakis, "Dose calculations for external photon beams in radiotherapy," Phys. Med. Biol. **44**, R99–R155 (1999).
[2] W. R. Nelson, H. Hirayama, and D. W. O. Rogers, "The EGS4 Code System," SLAC Report No. SLAC-265, 1985.

[3] J. S. Hendricks, ''A Monte Carlo code for particle transport,'' Los Alamos Sci. **22**, 30–43 (1994).
[4] J. Sempau, E. Acosta, J. Baró, J. M. Fernández-Varea, and F. Salvat, ''An algorithm for Monte Carlo simulation of coupled electron-photon showers,'' Nucl. Instrum. Methods Phys. Res. B **132**, 377–390 (1997).
[5] I. Kawrakow, ''Accurate condensed history Monte Carlo simulation of electron transport, I. EGSnrc, the new EGS4 version,'' Med. Phys. **27**, 485–498 (2000).
[6] H. Neuenschwander and E. Born, ''A macro Monte Carlo method for electron beam dose calculations,'' Phys. Med. Biol. **37**, 107–125 (1992).
[7] I. Kawrakow, M. Fippel, and K. Friedrich, ''3D electron dose calculation using a voxel based Monte Carlo algorithm (VMC),'' Med. Phys. **23**, 445–457 (1996).
[8] P. J. Keall and P. W. Hoban, ''An accurate 3-D x-ray dose calculation method combining superposition and pre-generated Monte-Carlo electron track histories,'' Med. Phys. **23**, 479–485 (1996).
[9] L. Wang, C. S. Chui, and M. Lovelock, ''A patient-specific Monte Carlo dose-calculation method for photon beams,'' Med. Phys. **25**, 867–878 (1998).
[10] M. Fippel, ''Fast Monte Carlo dose calculation for photon beams based on the VMC electron algorithm,'' Med. Phys. **26**, 1466–1475 (1999).
[11] I. Kawrakow and M. Fippel, ''Investigation of variance reduction techniques for Monte Carlo photon dose calculation using XVMC,'' Phys. Med. Biol. **45**, 2163–2183 (2000).
[12] J. Sempau, S. J. Wilderman, and A. F. Bielajew, ''DPM, a fast, accurate Monte Carlo code optimized for photon and electron radiotherapy treatment planning dose calculations,'' Phys. Med. Biol. **45**, 2263–2291 (2000).
[13] J. S. Li, T. Pawlicki, J. Deng, S. B. Jiang, E. Mok, and C. M. Ma, ''Validation of a Monte Carlo dose calculation tool for radiotherapy treatment planning,'' Phys. Med. Biol. **45**, 2969–2985 (2000).
[14] C. L. Hartmann Siantar, R. S. Walling, T. P. Daly, B. Faddegon, N. Albright, P. Bergstrom, C. Chuang, D. Garrett, R. K. House, D. Knapp, D. J. Wieczorek, and L. J. Verhey, ''Description and dosimetric verification of the PEREGRINE Monte Carlo dose calculation system for photon beams incident on a water phantom,'' Med. Phys. **28**, 1322–1337 (2001).
[15] D. M. J. Lovelock, C. S. Chui, and R. Mohan, ''A Monte Carlo model of photon beams used in radiation therapy,'' Med. Phys. **22**, 1387–1394 (1995).
[16] D. W. O. Rogers, B. A. Faddegon, G. X. Ding, C. M. Ma, J. Wei, and T. R. Mackie, ''BEAM: A Monte Carlo code to simulate radiotherapy treatment units,'' Med. Phys. **22**, 503–524 (1995).
[17] D. Sheikh-Bagheri and D. W. O. Rogers, ''Sensitivity of megavoltage photon beam Monte Carlo simulations to electron beam and other parameters,'' Med. Phys. **29**, 379–390 (2002).
[18] D. Sheikh-Bagheri and D. W. O. Rogers, ''Monte Carlo calculation of nine megavoltage photon beam spectra using the BEAM code,'' Med. Phys. **29**, 391–402 (2002).
[19] G. X. Ding, ''Energy spectra, angular spread, fluence profiles and dose distributions of 6 MV and 18 MV photon beams: Results of Monte Carlo simulations for a Varian 2100EX accelerator,'' Phys. Med. Biol. **47**, 1025–1046 (2002).
[20] C. M. Ma and S. B. Jiang, ''Monte Carlo modelling of electron beams from medical accelerators,'' Phys. Med. Biol. **44**, R157–R189 (1999).
[21] J. Deng, S. B. Jiang, A. Kapur, J. Li, T. Pawlicki, and C. M. Ma, ''Photon beam characterization and modelling for Monte Carlo treatment planning,'' Phys. Med. Biol. **45**, 411–427 (2000).
[22] A. E. Schach von Wittenau, P. M. Bergstrom, and L. J. Cox, ''Patient-dependent beam-modifier physics in Monte Carlo photon dose calculations,'' Med. Phys. **27**, 935–947 (2000).
[23] M. K. Fix, M. Stampanoni, P. Manser, E. J. Born, R. Mini, and P. Rüegsegger, ''A multiple source model for 6 MV photon beam dose calculations using Monte Carlo,'' Phys. Med. Biol. **46**, 1407–1427 (2001).
[24] A. Ahnesjö, T. Knöös, and A. Montelius, ''Application of the convolution method for calculation of output factors for therapy photon beams,'' Med. Phys. **19**, 295–301 (1992).
[25] P. B. Dunscombe and J. M. Nieminen, ''On the field-size dependence of relative output from a linear accelerator,'' Med. Phys. **19**, 1441–1444 (1992).
[26] A. Ahnesjö, ''Analytic modeling of photon scatter from flattening filters in photon therapy beams,'' Med. Phys. **21**, 1227–1235 (1994).
[27] M. B. Sharpe, D. A. Jaffray, J. J. Battista, and P. Munro, ''Extrafocal radiation: A unified approach to the prediction of beam penumbra and output factors for megavoltage x-ray beams,'' Med. Phys. **22**, 2065–2074 (1995).
[28] M. K. Yu and R. Sloboda, ''Analytical representation of head scatter factors for shaped photon beams using a two-component x-ray source model,'' Med. Phys. **22**, 2045–2055 (1995).
[29] T. C. Zhu and B. E. Bjärngard, ''The fraction of photons undergoing head scatter in x-ray beams,'' Phys. Med. Biol. **40**, 1127–1134 (1995).
[30] K. L. Lam, M. S. Muthuswamy, and R. K. Ten Haken, ''Flattening-filter-based empirical methods to parametrize the head scatter factor,'' Med. Phys. **23**, 343–352 (1996).
[31] P. A. Jursinic, ''Clinical implementation of a two-component x-ray source model for calculation of head-scatter factors,'' Med. Phys. **24**, 2001–2007 (1997).
[32] H. H. Liu, T. R. Mackie, and E. C. McCullough, ''A dual source photon beam model used in convolution/superposition dose calculations for clinical megavoltage x-ray beams,'' Med. Phys. **24**, 1960–1974 (1997).
[33] H. H. Liu, T. R. Mackie, and E. C. McCullough, ''Calculating output factors for photon beam radiotherapy using a convolution/superposition method based on a dual source photon beam model,'' Med. Phys. **24**, 1975–1985 (1997).
[34] T. C. Zhu, B. E. Bjärngard, Y. Xiao, and C. J. Yang, ''Modeling the output ratio in air for megavoltage photon beams,'' Med. Phys. **28**, 925–937 (2001).
[35] Y. Yang, L. Xing, A. L. Boyer, Y. Song, and Y. Hu, ''A three-source model for the calculation of head scatter factors,'' Med. Phys. **29**, 2024–2033 (2002).
[36] S. B. Jiang, A. L. Boyer, and C. M. Ma, ''Modeling the extrafocal radiation and monitor chamber backscatter for photon beam dose calculation,'' Med. Phys. **28**, 55–66 (2001).
[37] W. H. Press, S. A. Teukolsky, W. T. Vetterling, and B. P. Flannery, *Numerical Recipes in C* (Cambridge University Press, Cambridge, 1992).
[38] R. C. Tailor, V. M. Tello, C. B. Schroy, M. Vossler, and W. F. Hanson, ''A generic off-axis energy correction for linac photon beam dosimetry,'' Med. Phys. **25**, 662–667 (1998).
[39] A. Ahnesjö, M. Saxner, and I. Thorslund, ''Modelling of photon beam spectral variations,'' in XIII International Conference on the Use of Computers in Radiation Therapy (ICCR), Heidelberg, Germany, 2000.
[40] M. J. Berger and J. H. Hubbell, ''XCOM: Photon cross sections on a personal computer,'' Technical Report No. NBSIR 87-3597, National Institute of Standards and Technology Gaithersburg, MD, 1987.
[41] I. Kawrakow and D. W. O. Rogers, ''The EGSnrc code system: Monte Carlo simulation of electron and photon transport,'' NRCC Report No. PIRS-701, 2000.
[42] F. Haryanto, M. Fippel, W. Laub, O. Dohm, and F. Nüsslin, ''Investigation of photon beam output factors for conformal radiation therapy—Monte Carlo simulations and measurements,'' Phys. Med. Biol. **47**, N133–N143 (2002).